Biosensors and Bioelectronics 41 (2013) 424–429

Contents lists available at SciVerse ScienceDirect

Biosensors and Bioelectronics

journal homepage: www.elsevier.com/locate/bios

# Characterization of a modified gold platform for the development of a label-free anti-thrombin aptasensor

Yamile Jalit [a], Fabiana A. Gutierrez [a], Galina Dubacheva [b], Cedric Goyer [b], Liliane Coche-Guerente [b], Eric Defrancq [b], Pierre Labbé [b], Gustavo A. Rivas [a], Marcela C. Rodríguez [a,*]

[a] Instituto de Investigaciones en Físico Química de Córdoba (INFIQC) CONICET-UNC, Departamento de Físico Química, Facultad de Ciencias Químicas, Universidad Nacional de Córdoba, Ciudad Universitaria, 5000 Córdoba, Argentina
[b] DCM-Département de Chimie Moléculaire UMR CNRS 5250, ICMG FR-2607, Université Joseph Fourier BP-53 38041 Grenoble Cedex 9, France

ARTICLE INFO

*Article history:*
Received 20 June 2012
Received in revised form
24 August 2012
Accepted 31 August 2012
Available online 8 September 2012

*Keywords:*
Thrombin binding aptamer
Aptasensor
Optical aptasensor
Thrombin biosensor
Protein detection
SPR sensing

ABSTRACT

This work reports the characterization of a modified gold surface as a platform for the development of a label free aptasensor for thrombin detection. The biorecognition platform was obtained by the self-assembly of 4-mercaptobenzoic acid onto a gold surface, covalent attachment of streptavidin and further immobilization of the biotinylated anti-thrombin aptamer. The biosensing platform was characterized by cyclic voltammetry, electrochemical impedance spectroscopy, surface plasmon resonance (SPR) and quartz crystal microbalance with dissipation monitoring.

The biorecognition event aptamer-thrombin was detected from changes in the SPR angle produced as a consequence of the molecular interaction between the aptasensor and the target protein. The biosensing platform demonstrated to be highly selective for human thrombin even in the presence of large excess of bovine thrombin, bovine serum albumin, cytochrome C, lysozyme and myoglobin. The relationship between the changes in the SPR angle and thrombin concentration was linear up to 0.19 μmol $L^{-1}$ ($R^2$=0.992) while the detection limit was of 12.0 nmol $L^{-1}$ (240 fmol in the sample). This new sensing approach represents an interesting and promising alternative for the SPR-based quantification of thrombin.



## 1. Introduction

Since their discovery in the 90's (Ellington and Szostak, 1990; Tuerk and Gold, 1990) aptamers have demonstrated to be an important analytical tool for the development of several bioanalytical strategies (Zhou et al., 2012; Lee et al., 2012; Wu et al., 2012, Nam et al., 2012; Iliuk et al., 2011). Aptamers are artificial single strand nucleic acids (DNA or RNA) obtained by SELEX (Systematic Evolution of Ligands by EXponencial enrichment) iterative process based on the adsorption, recovery and re-amplification of artificial nucleic acids from a complex library (James, 2000). Numerous targets can be recognized by aptamers, ranging from cells and biomacromolecules to small molecules and ions (Strehlitz et al., 2012; Göringer, 2012; Lau and Li, 2011; Soontornworajit and Wang, 2011). The extended list of advantages exhibited by aptamers position them over antibodies in terms of the development of analitycal assays or devices (Zhou et al., 2012; Lee et al., 2012; Wu et al., 2012, Nam et al., 2012; Iliuk et al., 2011; James, 2000).

The association of thrombin and its corresponding thrombin binding aptamer is a model system for the development of sensing devices involving aptamers as recognition molecule. Thrombin is a serine protease with multifunctional purposes in addition to procoagulant and anticoagulant functions that recognizes a number of macromolecular substrates. It exposes two well-known electropositive exosites for the specific substrate interaction, the fibrinogen recognition exosite at the base of the active-site cleft and a more strongly electropositive exosite for heparin-binding (Tsiang et al., 1995; Tasset et al., 1997). While two thrombin-binding aptamers have been discovered recently, the earliest and widely studied aptamer has been the 15-mer DNA-aptamer 5′-GGTTGGTGTGGTTGG-3′ isolated by Bock et al., 1992. This aptamer folded tightly into a quadruplex structure that binds thrombin at the fibrinogen exosite (Tsiang et al., 1995). Several biosensing strategies for thrombin detection have been proposed including electrochemical, (Meini et al., 2012; Tang et al., 2012) colorimetric (Liang et al., 2011; Zhang et al., 2010), fluorescence (Wang Y. et al., 2011; Zheng et al., 2012), acoustic (Chen et al., 2010; Jung et al., 2007) thermal (Wang C. et al. 2012) and optical transduction systems (Zhu et al., 2012; Guo and Kim, 2012; Shevchenko et al., 2011). The optical detection strategies have gained great attention due to the real-time,

* Corresponding author. Tel. +54 351 4334169/80; fax: +54 351 4334188.
*E-mail address:* marcela.rodriguez@fcq.unc.edu.ar (M.C. Rodríguez).

0956-5663/$ - see front matter © 2012 Elsevier B.V. All rights reserved.
http://dx.doi.org/10.1016/j.bios.2012.08.061

label-free, high-sensitive and non-destructive operation mode, coupled with the versatility required for the quantification of different analytes of clinical relevance (Strehlitz et al., 2012; Sassolas et al., 2011). In the last 30 years surface plasmon resonance (SPR) has become one of the most successful optical approaches for the study of biomolecular affinity interactions and kinetics processes, allowing the development of sensors and biosensors (Fernández et al., 2012; Liu and Chen, 2012). The biomolecular interactions at the nanometer level take place in the layers contiguous to the interface; and the analytical signal that arises from the resulting changes in reflectivity is proportional to the mass of biomolecules bound to the surface (Feng et al., 2012; Cheng and Ming, 2012).

So far, most of the aptasensors based on the SAM strategy have used aliphatic thiolated compounds. Considering that the presence of aromatic groups in the thiol improves the performance of the resulting electrodes (Wang H. et al., 2011) and that the carboxylic group can be used for further covalent attachment of biomolecules (Nuzzo et al., 1990), 4-mercaptobenzoic acid (4MBA) can be used in the development of a suitable platform for aptasensor design. In this approach we take advantages of the 4MBA self-assembly and further modification by covalent attachment of streptavidin (SA) followed by the anchoring of a biotinylated thrombin binding aptamer (TBA). Even though, the affinity coupling biotin-SA has been used for aptamer anchoring strategy, here we introduce a new modification of the classical protocol (Li et al., 2008; Ostatná et al., 2008).

In this work, we are reporting for the first time an anti-thrombin aptasensor for the selective and sensitive detection of thrombin based on the use of a gold surface modified with a 4-mercaptobenzoic acid (4MBA) self-assembled monolayer (SAM). The system was characterized with Cyclic Voltammetry (CV), Electrochemical Impedance Spectroscopy (EIS), Quartz Crystal Microbalance with dissipation monitoring (QCM-D) and Surface Plasmon Resonance (SPR). The aptasensor reported here presents detection limits placed in the range of nmol $L^{-1}$ and dissociation constant values ($K_D$) that are comparable to those found in the literature. In the following sections we discuss the optimization of the surface modification steps and the analytical application of the proposed biosensor for thrombin quantification.

## 2. Material and methods

### 2.1. Reagents

4-mercaptobenzoic acid (4MBA), N-hydroxysuccinimide (NHS), 1-ethyl-3-(3-dimethylamino-propyl) carbodiimide (EDC), bovine serum albumin (BSA), ethanolamine hydrocloride ($EtOHNH_2$) and human-α-thrombin (MW=37.4 kDa) were obtained from Sigma. Streptavidin (SA, MW=60 kDa) were from Invitrogen Life Technologies. The biotinylated 15-mer DNA thrombin binding aptamer (TBA, MW=6956 Da) with a polyT tail used in this study has the following sequence:5′-biotin-TTT TTT GGT TGG TGT GGT TGG-3′, it was obtained either from Invitrogen Life Technologies or synthesized by Dr. Eriq Defrancq.

Absolute ethanol and sulfuric acid (98%) were provided by J. T. Baker. A solution of 0.020 mol $L^{-1}$ acetate buffer pH 5.00 was used for the SA attachment step; a solution of 0.050 mol $L^{-1}$ N-(2-hydroxyethil)piperazine-N′-2-ethansulfonic acid (HEPES) pH 7.40+NaCl 0.010 mol $L^{-1}$+KCl $5.0\times10^{-3}$ mol $L^{-1}$+$MgCl_2$ $1.0\times10^{-3}$ mol $L^{-1}$ was employed as interaction buffer (IB) for the aptamer, while 0.050 mol $L^{-1}$ HEPES pH 7.40+0.010 mol $L^{-1}$ NaCl+$5.0\times10^{-3}$ mol $L^{-1}$ KCl+$1.0\times10^{-3}$ mol $L^{-1}$ $MgCl_2$+0.010% Tween-20 was employed as washing buffer (WB). The detection buffer (DB) was 0.050 mol $L^{-1}$ phosphate buffer solution pH 7.40 likewise used as supporting electrolyte in cyclic voltammetry and electrochemical impedance spectroscopy measurements. Potassium ferricyanide $K_3[Fe(CN)_6]$ and ferrocyanide $K_4[Fe(CN)_6]$ were purchased from Merk and NBS Biological, respectively. Other chemicals were reagent grade and used without further purification. Ultrapure water (UW, $\rho=18.2$ MΩ cm) from a Millipore-MilliQ system was used for preparing all the solutions.

### 2.2. Apparatus

Cyclic voltammetric (CV) experiments were performed with a TEQ_04 potentiostat. The electrodes were inserted into the cell through holes in its Teflon cover. A platinum wire and Ag/AgCl, 3 mol $L^{-1}$ NaCl (BAS, Model RE-5B) were used as counter and reference electrodes, respectively. All potentials are referred to the latter. The experiments were carried out in a 0.050 mol $L^{-1}$ phosphate buffer solution pH 7.40, using $1.0\times10^{-3}$ mol $L^{-1}$ $K_3[Fe(CN)_6]$ as redox mediator. Cyclic voltammograms were recorded at 0.100 $Vs^{-1}$.

Electrochemical Impedance Spectroscopy (EIS) measurements were performed with a Solartron SI1287 coupled with FRA SI1260 software. The redox probe was 0.010 mol $L^{-1}$ $K_3[Fe(CN)_6]$/$K_4[Fe(CN)_6]$ in a 0.050 mol $L^{-1}$ phosphate buffer solution pH 7.40. The EIS parameters are the following: amplitude: 0.010 V, frequency range: $1.0\times10^{-2}$–$1.0\times10^{6}$ Hz and working potential: +0.200 V.

QCM-D measurements were performed using Q-Sense, E4 instrument (Q-Sense, AB, Göteborg, Sweden) equipped with axial flow chamber and polished AT-cut piezoelectric quartz crystals covered by 100 nm gold. Both frequency ($F$) and energy dissipation ($D$) changes of the quartz crystal regarding mass and structural properties of the adsorbed molecular layers, respectively, were measured at the fundamental resonance frequency (5 MHz) as well as at the third, fifth, seventh, ninth, eleventh, and thirteenth overtones ($n$=3, 5, 7, 9, 11 and 13). The measurements were performed at 24 °C. In the case of homogenous, quasi-rigid films (for which the change in dissipation is less than $10^{-6}$ per 5 Hz of $\Delta F$), the frequency shifts are proportional to the $\Delta m$ mass uptake per unit area that can be deduced from the Sauerbrey (1959) relationship Eq. (1):

$$\Delta m = -C\Delta F_n/n \quad (1)$$

where the mass sensitivity, $C$, is equal to 17.7 ng $cm^{-2}$ $Hz^{-1}$ at $f_1$=5 MHz.

Prior to use, the sensors crystals were exposed to a UV-ozone treatment for 5 min using UVO cleaner (Jelight Company) and immersed in ethanol under stirring for 20 min. Before the experiment was started, the resonance frequency and dissipation found for each overtone were set equal to zero. Experiments were conducted in a continuous flow of buffer with a flow rate of 50 μL.$min^{-1}$ by using a peristaltic pump (ISM935C, Ismatec, Zurich, Switzerland).

Surface Plasmon Resonance (SPR) measurements were performed using a single channel, AUTOLAB E-SPR SPRINGLE instrument (Eco Chemie, The Netherlands) and a standard sensor disk gold-coated glass (BK-7 Eco Chemie). The sensor disk was mounted on a hemicylindrical lens through index-matching oil to form the base of a cuvette. Sample solutions were injected manually into the cuvette. The measurements were carried out under batch conditions at 25 °C. The SPR angle shifts ($\Delta\theta$) were converted into mass uptake using a sensitivity factor of 120 m° corresponding to 100 ng $cm^{-2}$ of protein or ssDNA, and the MW of each immobilized molecule (Yang et al., 2007).

### 2.3. Preparation of the working electrodes:

#### 2.3.1. Self-assembled monolayer of 4MBA:

Polycrystalline gold electrodes (CH Instruments) were used as substrate. Prior to thiol modification, the electrodes were cleaned

using "*Piranha*-solution" (70% $H_2SO_4$–30% $H_2O_2$, ***Caution:*** *Piranha-solution must be handled with care. It is extremely oxidizing and reacts violently*). The electrodes were then polished with 1.0 μm alumina powder for 6 min. After polishing, the gold electrodes were cleaned with "*Piranha*-solution" and carefully rinsed with ultrapure water. The gold surface was then electrochemically pretreated in 0.50 mol $L^{-1}$ sulfuric acid solution until the expected profile was obtained. The electrode surface was thoroughly rinsed with UW, dried in a stream of $N_2$ and then immersed overnight in a $4.0 \times 10^{-3}$ mol $L^{-1}$ 4MBA ethanolic solution at room temperature.

*2.3.2. Construction of the biorecognition platform (Au/4MBA/SA/TBA):*

The biosensor was prepared in the following way: the 4MBA-modified-gold surface was rinsed with ethanol and UW prior to the next modification. The platform building-up process was carried out in a humidity chamber in order to keep a wet environment during the sensing platform construction stages. A mix of $200.0 \times 10^{-3}$ mol $L^{-1}$ EDC and 50.0 mol $L^{-1}$ NHS solution was dropped on top of the electrodes and incubated for 30 min. Then, the electrodes were washed with 0.020 mol $L^{-1}$ acetate buffer pH 5.00 followed by the addition of a 1.67 μmol $L^{-1}$ SA solution on top of the electrode for 60 min. The SA modified electrodes were rinsed with UW and blocked with 1.0 mol $L^{-1}$ $EtOHNH_2$ pH 8.50. The 14.4 μmol $L^{-1}$ TBA solution was heated at 90 °C for 3 min and then cooled in ice bath to obtain a proper folding configuration (Cai et al., 2006; Li et al., 2008). After this procedure, TBA was immobilized as the capture component of the aptasensor.

*2.3.3. Protein binding procedure*

An aliquot of 20 μL of thrombin solution was placed on top of the electrode surface for 30 min in a humidity chamber. Then, the aptasensor was rinsed with WB and placed into the cell to perform the given measurement.

The procedures in Sections 2.3.1, 2.3.2 and 2.3.3 were followed for the surface preparation either by SPR or QCM-D experiments.

## 3. Results and discussion

At variance with the general scheme used in other works, we evaluate the system using different techniques to obtain a complete knowledge of the bioanalytical platform and to improve its performance.

### 3.1. Electrochemical characterization

The construction of a suitable aptamer-based platform involves several steps. In this approach a gold electrode was used as initial surface for the anti-thrombin aptasensor fabrication through the self-assembling of 4MBA overnight, as it is shown in Scheme 1.

Reductive desorption of SAMs is a convenient method to estimate the surface concentration of adsorbed molecules. In order to know the surface coverage of 4MBA at different adsorption times (0.5, 1, 2, 3, 6, 9, 15 h), CV experiments were recorded from −0.200 V to −1.500 V at 0.100 $Vs^{-1}$ in 0.10 mol $L^{-1}$ NaOH for unmodified and 4MBA-modified-gold electrodes. The response obtained for 4MBA-modified gold electrode (in contrast to the unmodified one) shows a cathodic peak current at −0.9 V approximately, which is associated to the monolayer electrodesorption process and it was used to obtain the surface coverage (data not shown). Although there is no difference in surface coverage with the increase of adsorption time, it is known that longer times result in an ordered and more stable film. In the case of aromatic thiols this fact is mainly due to the establishment of the π-stacking interaction throughout the aromatic rings of the molecules (Love et al., 2005). Consequently, 15 h was chosen as an optimal time for thiol adsorption. Under these conditions, the surface coverage was $6.0 \times 10^{-10}$ mol $cm^{-2}$, in agreement with previous reports (Sawaguchi et al., 2000; Taniguchi et al., 2003).

The optimal time for SA immobilization was selected from CV experiments using $K_3[Fe(CN)_6]$ $1.0 \times 10^{-3}$ mol $L^{-1}$ as redox indicator (prepared in DB). Fig. S1 of Supporting information (SI) shows the peak potential separation ($\Delta E_p$) of the redox marker obtained from CV experiments at gold electrodes modified with 4MBA and SA covalently attached (Au/4MBA/SA) after different reaction times (30, 60, 90 and 120 min). When immobilizing SA there are two effects that have to be considered: the reversion of the negative charge of the thiol and the blocking effect for charge transfer. $\Delta E_p$ decreases with the increase in the immobilization time of SA, reaching the minimum value at 60 min ($\Delta E_p = (0.196 \pm 0.006)$ V). For those times, it is also possible the re-organization of the SA layer generating holes or pores that allow the diffusion of the redox probe contributing in this way to the decrease of the $\Delta E_p$. For interaction times longer than 90 min the $\Delta E_p$ starts to increase probably due to the formation of a more compact protein layer that makes difficult the diffusion and electron transfer process of the redox probe. Therefore, the selected time for further experiments was 60 min.

The immobilization time of TBA at Au/4MBA/SA was evaluated using EIS, a useful technique to follow biorecognition events by monitoring the changes in electron-transfer resistance ($R_{et}$) of a given probe (Katz and Willner, 2003). Fig. S2 (SI) shows the Nyquist plots of Au/4MBA/SA for different binding times of TBA (15, 30, 60 and 90 min). The Randles circuit (inset Fig. S2, SI) fitted the data obtained. The $R_{et}$ were employed as the analytical signal. After 15 min binding there is an increase of the $R_{et}$ compared to the initial SA layer due to the repulsion between the redox probe

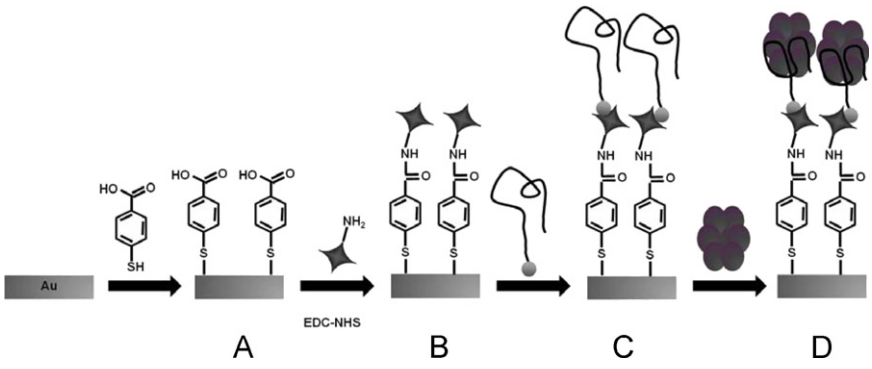


**Scheme 1.** Illustration of the aptasensor design. (A) 4MBA self-assembly; (B) covalent attachment of SA; (C) TBA immobilization onto SA layer; (D) thrombin detection.

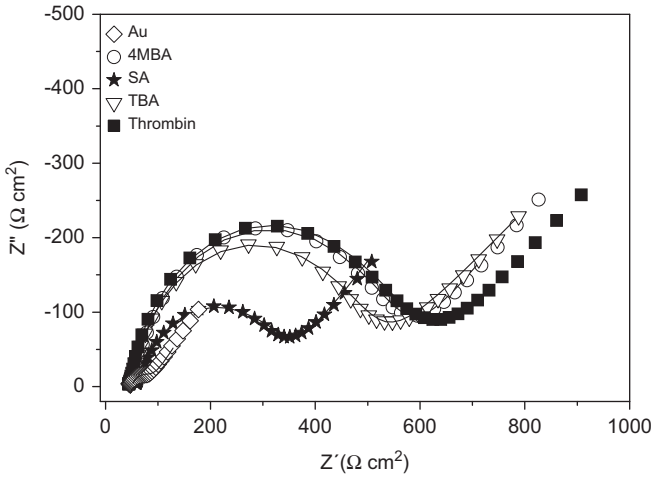


**Fig. 1.** Nyquist plot of 0.010 mol $L^{-1}$ $K_3[Fe(CN)_6]/K_4[Fe(CN)_6]$ in DB for the different stages during the aptasensor construction and thrombin detection. Frequency range: $1.0\times10^{-2}$–$1.0\times10^{6}$ Hz, modulation amplitude: 0.010 V, working electrode potential: +0.200 V.

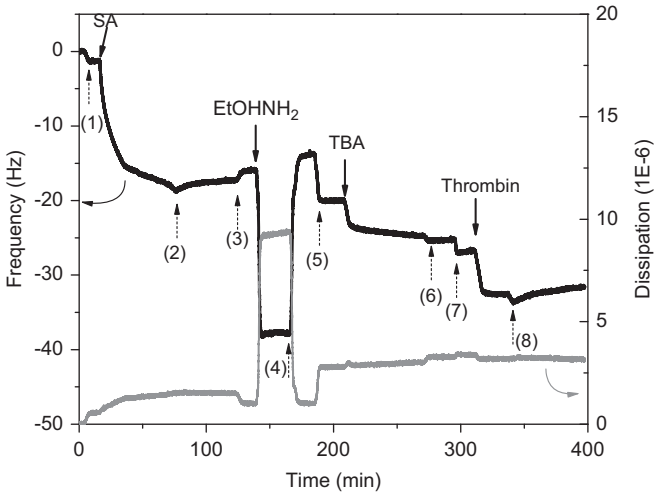


**Fig. 2.** QCM-D profile (frequency in black line and dissipation in grey line) obtained during the building of the biomolecular layer on the activated 4MBA-SAM (only the frequency and dissipation shifts for the seventh overtone are presented). Solid arrows correspond to the injections while dashed arrows, to washing steps (from time zero in UW to the end of the experiment: (1) and (2): acetate buffer; (3) and (4): UW; (5) and (6): IB; (7) and (8): WB).

and the negatively charged DNA-aptamer. The $R_{et}$ increases for 30 and 60 min reaching a constant value at higher times due to the saturation of the SA available sites. Therefore, 60 min was selected as the optimum time for further work.

Fig.1 shows the Nyquist plots obtained during the preparation of the bioanalytical platform. These profiles confirm the trend observed in CV experiments (see in Table S1 (SI) the values of $\Delta E_p$ and $R_{et}$ obtained from CV and EIS experiments). The gold electrode surface denoted a very low $R_{et}$ value ($(44\pm1)\,\Omega\,cm^2$) and $\Delta E_p=(0.071\pm0.002)$ V. The $R_{et}$ and $\Delta E_p$ values change with the platform modification progress. For 4MBA layer the $R_{et}$ enhances around 10 times ($(44\pm7)\times10^1\,\Omega\,cm^2$) and $\Delta E_p$ increases up to $(0.33\times0.01)$ V, showing the effect of two contributions, one of them related to a surface partial blocking effect and the other one associated to the high repulsion established between the negative charges of 4MBA and the redox probe. After the immobilization of SA layer the $R_{et}$ and $\Delta E_p$ decayed to ($(27\pm1)\times10^1\,\Omega\,cm^2$) and $(0.196\pm0.006)$ V, respectively, mainly due to the partial neutralization of the 4MBA negative charges. After the incorporation of TBA, the $R_{et}$ and $\Delta E_p$ increase up to ($(42\pm4)\times10^1\,\Omega\,cm^2$) and $(0.32\pm0.03)$ V respectively. This effect is mostly due to the repulsion between the ssDNA-backbone and the redox probe which implies an apparent decrease of the electron transfer rate, evidencing the efficiency in TBA immobilization. In order to test the binding capacity for thrombin of the Au/4MBA/SA/TBA, it was challenged with $2.67\times10^{-7}$ mol $L^{-1}$ thrombin. Fig. 1 and Table S1 (SI) show the increase of $R_{et}$ up to $(50\pm6)\times10^1\,\Omega\,cm^2$ when thrombin is bound, demonstrating that Au/4MBA/SA/TBA could be used as a suitable platform for thrombin detection. It is important to mention that even when CV and EIS give similar information, EIS is more sensitive and allows discriminating small $R_{et}$ changes upon the target recognition (Table S1, SI).

### 3.2. QCM-D and SPR characterization

QCM-D and SPR are useful for the study of biomolecular binding events. It is important to remark that QCM-D measures the molar mass of the adsorbed molecules together with the associated water (data shown in SI). The contribution of water to the total mass is not easy to substract, nevertheless, QCM-D is helpful for obtaining the properties of any mass coupled to the quartz crystal. The water content could be obtained by comparison with SPR mass (SI). As it can be seen in Fig. 2, the growth of the platform could be monitored in real time, showing the changes in frequency and dissipation (for clarity, only the seventh overtone is presented). The recording of QCM-D profile starts just after the activation of the 4MBA layer using EDC–NHS. The immobilization of SA and TBA show slight increases in dissipation energy ($\Delta D=0.9\times10^{-6}$ and $\Delta D=0.47\times10^{-6}$, respectively). Therefore, the frequency measurements can be directly converted to mass using the Sauerbrey equation Eq.(1). The mass uptakes obtained were: $(28\pm2)\times10^1$ ng $cm^{-2}$ for SA and $(94\pm9)$ ng $cm^{-2}$ for TBA, respectively. The injection of thrombin results in a decrease in frequency corresponding to the increase of the sensor mass due to the TBA-thrombin interaction leading to a mass uptake of $(86\pm2)$ ng $cm^{-2}$. In parallel, a decrease in dissipation was observed, attributed to the formation of a rigid film upon the binding of the target protein.

In order to evaluate the specificity of the interaction of TBA with Au/4MBA/SA we compare the QCM-D response for a non-biotinylated aptamer. The injection of the unmodified-aptamer results in a very slight negative drive of the frequency, exhibiting a negligible non-specific adsorption onto the Au/4MBA/SA platform (Fig. S3, SI). When thrombin is added onto the Au/4MBA/SA/unmodified-aptamer, a very slight decrease in frequency is observed with a mass uptake of $(15\pm4)$ ng $cm^{-2}$, while onto Au/4MBA/SA/TBA the addition of thrombin leads to a mass uptake of $(86\pm2)$ ng $cm^{-2}$. From these results, it is possible to conclude that TBA immobilization ($(94\pm9)$ ng $cm^{-2}$) is mediated by SA-biotin interaction without non-specific adsorption, and that the capture of thrombin onto Au/4MBA/SA/TBA is favoured by the high affinity interaction of TBA towards thrombin coupled with the high orientation of TBA layer.

SPR is an appropriate tool for monitoring the construction and recognition event of a biosensing platform in real-time, allowing to obtain a label-free quantitative analysis. This technique is based on changes of SPR angle due to the specific molecular binding and exhibits a high sensitivity, making possible the discrimination between bound and un-bound molecules (Strehlitz et al., 2012). Fig. 3 displays a typical SPR sensorgram for monitoring the building of the platform. The gold sensor disk modified with 4MBA was set up on the measurement chamber and lately modified with SA and TBA in the usual mode. The SA immobilization results in a binding signal of $(11\pm1)\times10^1$ m°

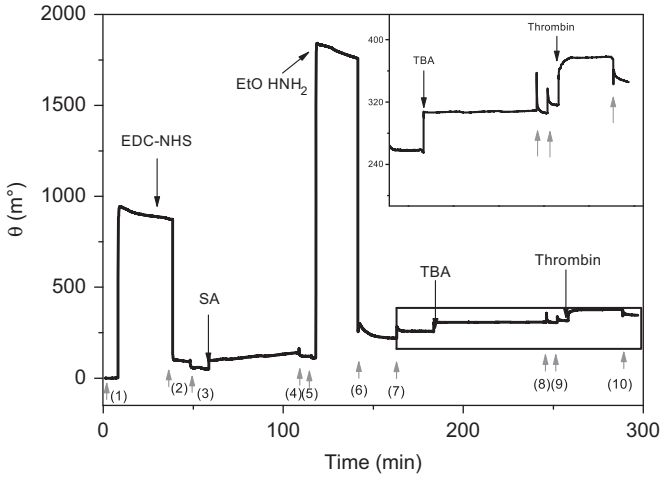


**Fig. 3.** SPR profile during the building of the biomolecular layer in real time. Black arrows correspond to the injections while grey arrows, to washing steps: (1) and (2): UW; (3) and (4): acetate buffer; (5) and (6): UW; (7) and (8): IB; (9) and (10): WB.

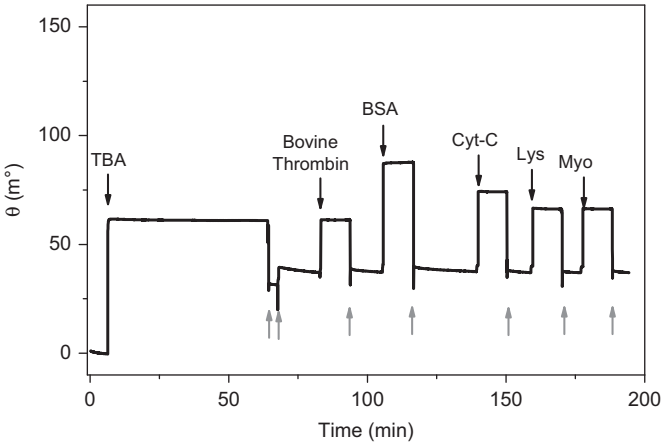


**Fig. 4.** SPR profile for the aptasensor after the injection of: 0.27 μmol $L^{-1}$ bovine thrombin, 0.15 μmol $L^{-1}$ BSA, 0.81 μmol $L^{-1}$ Cyt-C, 0.70 μmol $L^{-1}$ Lys and 0.58 μmol $L^{-1}$ Myo. The black arrows correspond to the injections while grey arrows, to washing steps with WB.

corresponding to $(1.4 \pm 0.3)$ pmol $cm^{-2}$. The anchoring of TBA presents a binding signal of $(27 \pm 5)$ m° that corresponds to $(3.1 \pm 0.5)$ pmol $cm^{-2}$. According to these results, the ratio TBA/SA is 2.3. Taking into account that SA molecules are immobilized through one or more amine-groups of the lysine residues with a random orientation is not surprising that the amount of TBA strands is approximately twice the amount of SA molecules under the working conditions. This observation is consistent with results reported by Knoll et al. for lower coverage when SA is covalently attached to mercaptoundecanoic acid (MUA) (Su et al., 2005). As a result of the steric hindrance effects, when the SA surface coverage is low, the spatially scattered SA molecules leave most of the available biotin binding sites accessible for the biotinylated aptamer interaction.

Regarding the biorecognition process, once the aptamer is immobilized, the interaction with $2.67 \times 10^{-7}$ mol $L^{-1}$ thrombin produces a change of $(7 \pm 1) \times 10^{1}$ m°, corresponding to $(1.6 \pm 0.2)$ pmol $cm^{-2}$. Thus, the ratio TBA/thrombin obtained was 1.9. This result indicates that only the half of TBA molecules is available for the target capture owe to steric hindrance for the accessibility of the protein (Tang et al., 2007).

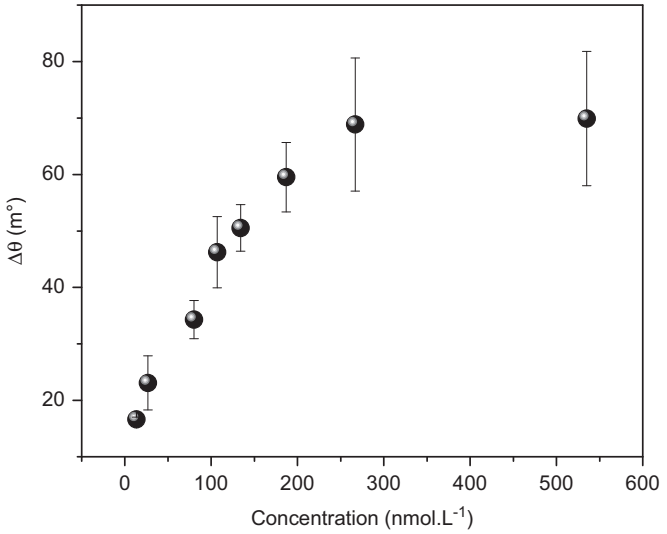


**Fig. 5.** Calibration plot for thrombin. Other conditions as in Fig. 3.

### 3.3. Analytical performance of the SPR-based aptasensor

In order to evaluate the aptasensor selectivity, the platform was challenged with high concentrations of different proteins. Fig. 4 displays a sensorgram for the aptamer-modified platform in the presence of 0.27 μmol $L^{-1}$ bovine thrombin, 0.15 μmol $L^{-1}$ bovine seric albumin (BSA), 0.81 μmol $L^{-1}$ cytochrome C (Cyt-C), 0.70 μmol $L^{-1}$ lysozyme (Lys) and 0.58 μmol $L^{-1}$ myoglobin (Myo). After the addition of bovine thrombin and washing, the signal returns to the baseline, revealing that there is no interaction between this protein and TBA, which is specific for human thrombin (Gopinath, 2008) even when bovine thrombin shows 85% homology compared to human thrombin (Liu et al., 2004). Au/4MBA/SA/TBA was challenged with 0.27 μmol $L^{-1}$ human thrombin, 0.15 μmol $L^{-1}$ BSA, 0.81 μmol $L^{-1}$ Cyt-C, 0.70 μmol $L^{-1}$ Lys and 0.58 μmol $L^{-1}$ Myo demonstrating that Au/4MBA/SA/TBA does not show non-specific interaction with proteins. In contrast, after the addition of human thrombin and further washing, the baseline signal changes proving the established recognition event of the human thrombin. According to Fig. 4 and Fig. S4 (SI), the aptasensor demonstrates its suitability for detecting and quantifying human thrombin accurately even in presence of high concentrations of proteins.

Fig. 5 depicts the calibration plot for the quantification of human thrombin. The variation of SPR signal ($\Delta\theta$) increases linearly with the increment in the concentration of human thrombin up to 0.19 μmol $L^{-1}$, reaching saturation values for concentrations higher than 0.27 μmol $L^{-1}$. After this value there is no appreciable signal changes due to the saturation with human thrombin molecules ($(1.6 \pm 0.2)$ pmol $cm^{-2}$). Even when the available TBA molecules are the double of the number of human thrombin molecules that could be immobilized until saturation, the inability for capturing more human thrombin molecules is related to the steric hindrance for the protein accessibility to the free-TBA. The calibration curve shows a linear regression of $\Delta\theta$ (m°) = 0.283 C (nmol $L^{-1}$) + 12.9, $R^2 = 0.992$. The aptasensor exhibits a detection limit of 12 nmol $L^{-1}$ (240 fmol in the sample) calculated as the ratio of 3.3 times the noise standard deviation and sensitivity of the calibration curve. This value is comparable to those reported recently in the literature for SPR based anti-thrombin aptasensors (Shevchenko et al., 2011; Henseleit et al., 2011; Ostatná et al., 2008). Therefore,

the developed aptasensor provides an easy, fast and highly sensitive way to quantify thrombin. In order to determine the $K_D$, the experimental data obtained were fitted considering one site binding model with the Langmuir adsorption isotherm $y=A_1x/(K_D+x)$, where $A_1$ is the saturation condition (Gronewold et al., 2005). This model was applied assuming that only one thrombin molecule was bound per TBA molecule. The fitted parameter values were $K_D$: $(43\pm3)$ nmol $L^{-1}$; $A_1$: $(70\pm3)$ m° and $R^2$: 0.985. It is important to notice that $K_D$ strongly depends on the experimental conditions and its value is consistent with those reported in the literature (from 20 up to 200 nmol $L^{-1}$) by Hianik et al., (2007): $(39\pm27)$ nmol $L^{-1}$ and Shevchenko et al., (2011): $(40\pm1)$ nmol $L^{-1}$.

## 4. Conclusions

This work reports a new modified platform for the development of an anti-human thrombin aptasensor based on the use of a gold surface modified with a 4-mercaptobenzoic acid (4MBA) self-assembled monolayer (SAM), SA and TBA. In terms of electrochemical characterization, the biorecognition layer was studied through the changes of the CV signal of $K_3[Fe(CN)_6]$ and the $R_{et}$ of the electrochemical probe ($K_3[Fe(CN)_6]/K_4[Fe(CN)_6]$) from EIS experiments. By using SPR, the sensitive thrombin detection was possible at the level of fmol in the sample. Excellent selectivity was accomplished with a proper control of the working conditions even in presence of high concentration of interferents, including the excellent discrimination between bovine and human thrombin.

Thus, the association between the molecular recognition properties of aptamers and modified gold-transducers make possible to obtain highly sensitive and selective SPR-based aptasensors allowing the development of new accurate devices for proteins detection.

## Acknowledgments

The authors thank CONICET, SECyT-UNC, ANPCyT (PICT-2010 1549), MINCyT-Córdoba and ECOS SUD-A08E04 for the financial support. Y.J. acknowledges the CONICET fellowship. The authors also want to thank to Ms. M.S. Vitali from Laboratorio de Hemoderivados (Universidad Nacional de Córdoba) for providing bovine thrombin.

## Appendix A. Supporting information

Supplementary data associated with this article can be found in the online version at http://dx.doi.org/10.1016/j.bios.2012.08.061.

## References

Bock, L.C., Griffin, L.C., Latham, J.A., Vermaas, E.H., Toole, J.J., 1992. Nature 355, 564–566.
Cai, H., Lee, T.M.-H., Hsing, I.-M., 2006. Sensors and Actuators B 114, 433–437.
Chen, Q., Tang, W., Wang, D., Wu, X., Li, N., Liu, F., 2010. Biosensors and Bioelectronics 26, 575–579.
Cheng, Y., Ming, H., 2012. Photonic Sensors 2, 37–49.
Ellington, A.D., Szostak, J.W., 1990. Nature 346, 818–822.
Feng, J., Siu, V.S., Roelke, A., Mehta, V., Rhieu, S.Y., Tayhas, G., Palmore, R., Pacifici, D., 2012. Nano letters 12, 602–609.
Fernández, F., Sánchez-Baeza, F., Marco, M.-P., 2012. Biosensors and Bioelectronics 34, 151–158.
Gopinath, S.C.B., 2008. Thrombosis Research 122, 838–847.
Göringer, H.U., 2012. Trends in Parasitology 28, 106–113.
Gronewold, T.M.A., Glass, S., Quandt, E., Famulok, M., 2005. Biosensors and bioelectronics 20, 2044–2052.
Guo, L., Kim, D.-H., 2012. Biosensors and Bioelectronics 31, 567–570.
Henseleit, A., Schmieder, S., Bley, T., Sonntag, F., Schilling, N., Quenzel, P., Danz, N., Klotzbach, U., Boschke, E., 2011. Engineering in Life Sciences 11, 573–579.
Hianik, T., Ostatná, V., Sonlajtnerova, M., Grman, I., 2007. Bioelectrochemistry 70, 127–133.
Iliuk, A.B., Hu, L., Tao, W.A., 2011. Analytical Chemistry 83, 4440–4452.
James, W., 2000. Aptamers. In: Meyers, R.A. (Ed.), Encyclopedia of Analytical Chemistry. John Wiley & Sons Ltd., Chichester, pp. 4848–4871.
Jung, A., Gronewold, T.M.A., Tewes, M., Quandt, E., Berlin, P., 2007. Sensors and Actuators B 124, 46–52.
Katz, E., Willner, I., 2003. Electroanalysis 15, 913–947.
Lau, P.S., Li, Y., 2011. Current Organic Chemistry 15, 557–575.
Lee, S., Song, K.-M., Jeon, W., Jo, H., Shim, Y.-B., Ban, C., 2012. Biosensors and Bioelectronics 35, 291–296.
Li, X., Shen, L., Zhang, D., Qi, H., Gao, Q., Ma, F., Zhang, C., 2008. Biosensors and Bioelectronics 23, 1624–1630.
Liang, G., Cai, S., Zhang, P., Peng, Y., Chen, H., Zhang, S., Kong, J., 2011. Analytica Chimica Acta 689, 243–249.
Liu, X., Cao, G., Ding, H., Zhang, D., Yang, G., Liu, N., Fan, M., Shen, B., Shao, N., 2004. FEBS Letters 562, 125–128.
Liu, Y., Chen, Q., 2012. Analytical Chemistry 84, 3179–3186.
Love, J.C., Estroff, L.A., Kriebel, J.K., Nuzzo, R.G., Whitesides, G.M., 2005. Chemical Reviews 105, 1103–1169.
Meini, N., Farre, C., Chaix, C., Kherrat, R., Dzyadevych, S., Jaffrezic-Renault, N., 2012. Sensors and Actuators B 166–167, 715–720.
Nam, E.J., Kim, E.J., Wark, A.W., Rho, S., Kim, H., Lee, H.J., 2012. Analyst 137, 2011–2016.
Nuzzo, R.G., Dubois, L.H., Allara, D.L., 1990. Journal of the American Chemical Society 112, 558–569.
Ostatná, V., Vaisocherová, H., Homola, J., Hianik, T., 2008. Analytical and bioanalytical chemistry 391, 1861–1869.
Sassolas, A., Blum, L.J., Leca-Bouvier, B.D., 2011. Biosensors and Bioelectronics 26, 3725–3736.
Sauerbrey, G., 1959. Zeitschrift für Physik 155, 206–222.
Sawaguchi, T., Mizutani, F., Yoshimoto, S., Taniguchi, I., 2000. Electrochimica Acta 45, 2861–2867.
Shevchenko, Y., Francis, T.J., Blair, D.A.D., Walsh, R., Derosa, M.C., Albert, J., 2011. Analytical chemistry 83, 7027–7034.
Soontornworajit, B., Wang, Y., 2011. Analytical and Bioanalytical Chemistry 399, 1591–1599.
Strehlitz, B., Reineman, C., Linkorn, S., Stoltenburg, R., 2012. Bioanalytical Reviews 4, 1–30.
Su, X., Wu, Y.-J., Robelek, R., Knoll, W., 2005. Langmuir 21, 348–353.
Tang, J., Tang, D., Niesser, R., Knopp, D., Chen, G., 2012. Analytica Chimica Acta 720, 1–8.
Tang, Q., Su, X., Loh, K.P., 2007. Journal of Colloid and Interface Science 315, 99–106.
Taniguchi, I., Ishimoto, H., Tazaki, M., 2003. Electrochemistry Communications 5, 857–861.
Tasset, D.M., Kubik, M.F., Steiner, W., 1997. Journal of Molecular Biology 272, 688–698.
Tsiang, M., Jain, A.K., Dunn, K.E., Rojas, M.E., Leung, L.L.K., Gibbs, C.S., 1995. The Journal of Biological Chemistry 270, 16854–16863.
Tuerk, C., Gold, L., 1990. Science 249, 505–510.
Wang, C., Hossain, M., Ma, L., Ma, Z., Hickman, J.J., Su, M., 2012. Biosensors and Bioelectronics 26, 437–443.
Wang, H., Ohnuki, H., Endo, H., Izumi, M., 2011. Physics Procedia 14, 2–6.
Wang, Y., Bao, L., Liu, Z., Pang, D.-W., 2011. Analytical Chemistry 83, 8130–8137.
Wu, Y., Zhan, S., Wang, F., He, L., Zhi, W., Zhou, P., 2012. Chemical Communications 48, 4459–4461.
Yang, N., Su, X., Tjong, V., Knoll, W., 2007. Biosensors and Bioelectronics 22, 2700–2706.
Zhang, Z., Wang, Z., Wang, X., Yang, X., 2010. Sensors and Actuators B 147, 428–433.
Zheng, D., Zhou, R., Lou, X., 2012. Analytical Chemistry 84, 3554–3560.
Zhou, M., Liu, Y., Tao, G., Yan, J., 2012. Biosensors and Bioelectronics 35, 489–492.
Zhu, D., Luo, J., Rao, X., Zhang, J., Cheng, G., He, P., Fang, Y., 2012. Analytica Chimica Acta 711, 91–96.